Supplementary Information

Super-Nernstian Ion Sensitive Field-Effect Transistor Exploiting Charge Screening in WSe_2/MoS_2 Heterostructure

Sooraj Sanjay[ǂ], *Mainul Hossain*[§], *Ankit Rao*[ǂ], *and Navakanta Bhat*[ǂ*]

[ǂ]Centre for Nano Science and Engineering, Indian Institute of Science, Bengaluru, India. [§]Department of Electrical and Electronic Engineering, University of Dhaka, Dhaka-1000, Bangladesh.

Supplementary Figures

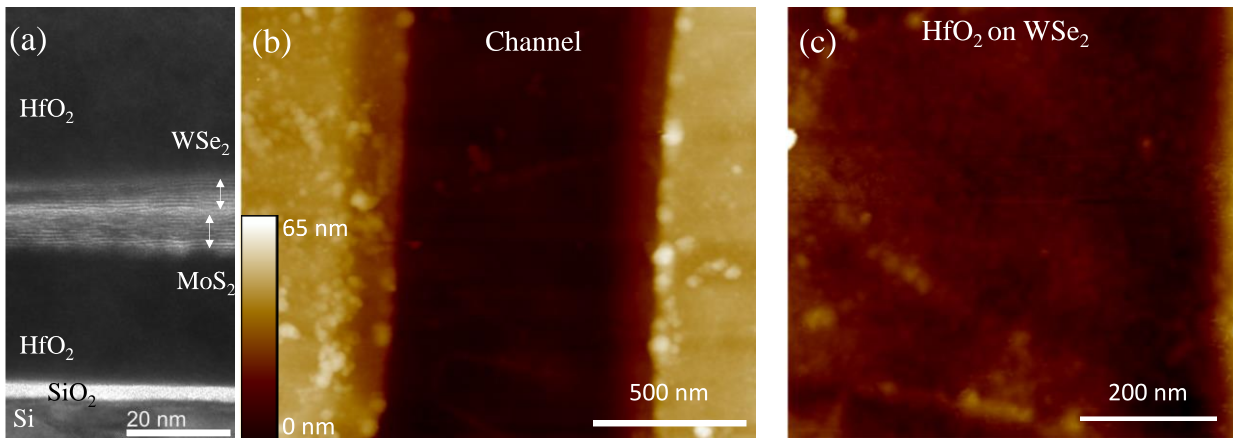

Supplementary Figure 1. Physical characteristics of device and dielectric. (a) HR-TEM of device cross section (channel region) showing excellent quality of top and bottom HfO_2 dielectrics (b) Atomic force microscopy (AFM) on the fabricated device after top HfO_2 deposition showing source, channel and drain regions, (c) AFM on the HfO_2 deposited over the top WSe_2 channel showing good uniformity of deposition with no island formation

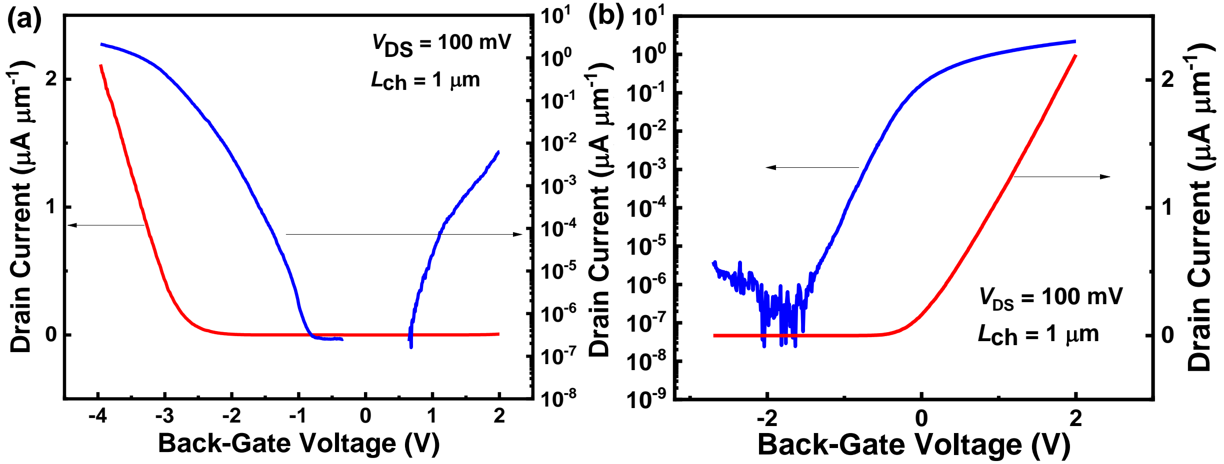

Supplementary Figure 2. Dry transfer characteristics of individual back-gated FETs using 30 nm HfO_2 dielectric. (a) back-gated WSe_2 FET with Pd contacts, (b) back-gated MoS_2 FET with Ni contacts.

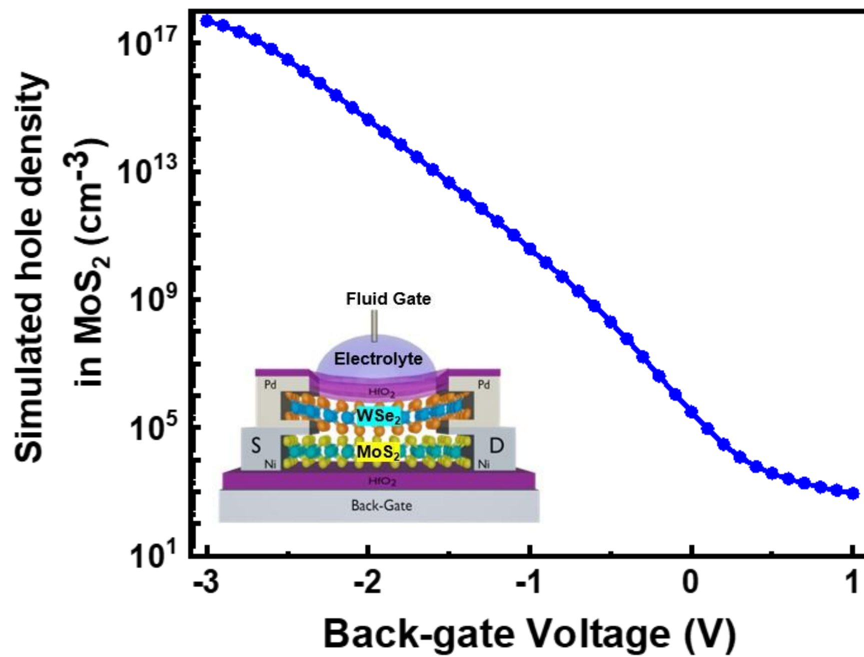

Supplementary Figure 3. Simulation of inversion carrier (hole) density in bottom MoS_2 layer, against back-gate voltage. This confirms the role of bottom MoS_2 layer in screening the top WSe_2 layer in the WSe_2(top)/MoS_2(bottom) ISFET.

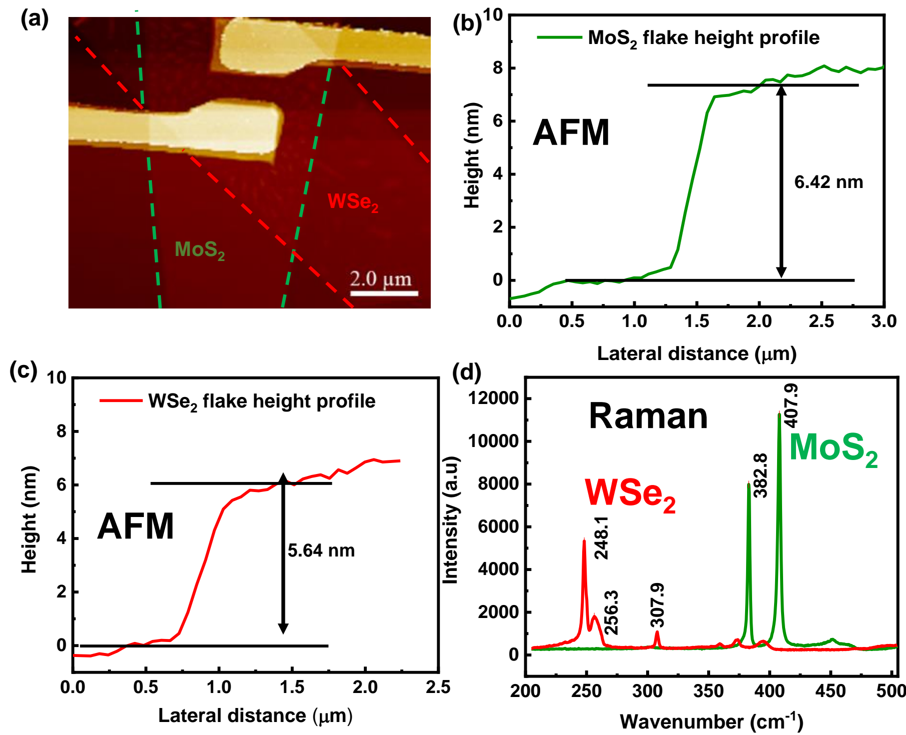

Supplementary Figure 4. **Characteristics of the exfoliated flakes.** (a) AFM image showing a WSe_2 flake stacked on top of a MoS_2 flake. Step heights of (b) MoS_2 and (c) WSe_2 flakes obtained from AFM measurement (d) Raman spectroscopy on MoS_2 and WSe_2 flakes. MoS_2 is identified by prominent vibrational modes at 382.8 cm-1 (E^1_{2g}) and 402.7 cm-1 (A_{1g}). Similarly, WSe_2 is marked by modes at 248.1 cm-1 (E^1_{2g}) and 256.3 cm-1(A_{1g}) and an additional peak at 307.9 cm-1, representing multi-layered flakes.[1]

Parameter	Back Dielectric	Top Dielectric
Thickness (from HR-TEM)	29.6 nm	33.7 nm
Roughness (from AFM)	0.516 nm (On Si)	0.784 – 1 nm (On WSe_2)
Dielectric Constant (from MOS Capacitor C-V)	~ 14	~14

Supplementary Table 1. Physical characteristics of the top and bottom HfO_2 dielectric. The thickness of the HfO_2 films were obtained from cross-section HR-TEM of the device. The thickness of bottom dielectric also includes 1-2 nm native oxide on silicon substrate. The rms roughness were all obtained from the AFM measurements on top and bottom dielectrics. The dielectric constant was determined using capacitance measurements on separate samples using metal oxide semiconductor (MOS) capacitors.

Parameter	Symbol	MoS_2	WSe_2	Reference
Bandgap (eV)	E_g	1.2	1.25	[2]
Effective mass of electrons	m_e^*/m_o	0.51	0.39	[3]
Effective mass of holes	m_p^*/m_o	0.66	0.51	[3]
Electron affinity (eV)	χ	4.2	3.9	[4]
Dielectric constant	k	6.9	7.8	[5,6]
Density of States (cm^{-3})	N_C, N_V	7.5×10^{20}	1.35×10^{20}	-
Doping concentration (cm^{-3})	*n, p*	10^{16} (n-type)	10^{16}(p-type)	-
Schottky barrier (eV)	φ	0.13	0.2	[7,8]
Arora model mobility (cm^2/V.s)	μ_{1n}, μ_{1p}	$\mu_{1n} = 420$	$\mu_{1p} = 520$	[9,10]
Arora model mobility (cm^2/V.s)	μ_{2n}, μ_{2p}	$\mu_{2n} = 83$	$\mu_{2p} = 150$	[9,10]
Contact Resistance ($k\Omega\ \mu m$)	R_C	2	12	-

Supplementary Table 2. Material and device parameters used in the TCAD simulation. The material parameters such as bandgap, effective mass, electron affinity and density of states were obtained from literature or calculated from other known parameters. Other parameters from the table were varied from an initial value (from literature or experiment) to calibrate with the experiment data. The final arrived values of parameters are given in the table.

Interface	Trap type	Energy level (eV)	Trap Density (cm^{-2})
HfO_2 – MoS_2	Acceptor	0.13 eV from CBE	1.5×10^{12}
HfO_2 – MoS_2	Acceptor	0.25 eV from CBE	1.0×10^{11}
MoS_2 – WSe_2	Donor	0.44 eV from VBE	3.0×10^{11}
MoS_2 – WSe2	Donor	0.34 eV from VBE	1.0×10^{12}
MoS_2 – WSe_2	Donor	0.26 eV from VBE	3.4×10^{12}

Supplementary Table 3. Interface trap densities used in the TCAD simulation. Interface traps were introduced at HfO_2-MoS_2 and MoS_2-WSe_2 interfaces to match the experiment and simulation transfer characteristics. Here, CBE is Conduction Band Edge and VBE is Valence Band Edge.

Supplementary Notes

Electrolyte Modeling for TCAD Simulation

The ions in an electrolyte obey the Poisson Botzmann distribution. The equation corresponding to a symmetric monovalent electrolyte is given in equation 1; where c_0^+, c_0^- are cation and anion concentrations, ε is the permittivity of water, φ is the potential in the solution, and x is the distance from the interface to bulk of solution.[11] The fermi dirac statistics followed by carriers in a semiconductor can also be approximated by a similar Boltzmann equation when the semiconductor

operates in non-degenerate state. Hence, the electrolyte solution is mimiced using an intrinsic semiconductor material with the relative permittivity of water ($\varepsilon \approx 80\varepsilon_0$).The bandgap E_g is kept large (5 eV) to ensure the semiconductor behaves as non-degenerate at all biases and behave identical to ions in the electrolyte. Although this model represents a monovalent symmetric electrolyte, it can be extended to multivalent systems with reasonable accuracy by introducing suitable correction factors to the density of states.[12] The pH of the electrolyte is modeled as a change in the effective density of states (N_C, N_V) determined for any given pH using the equations 2 and 3 given below; where N_A is the Avogadro number, E_g is the bandgap of the semiconductor, k_B is the Boltzmann constant and T is the temperature.[11] Every other parameter of the semiconductor uses the default of silicon.

$$\frac{\partial^2 \varphi}{\partial x^2} = -\frac{q}{\varepsilon}\left\{c_0^+ e^{-\frac{q\varphi}{k_B T}} - c_0^- e^{\frac{q\varphi}{k_B T}}\right\} \tag{1}$$

$$N_C = 10^{-14+pH}\, N_A\, 10^{-3} e^{\frac{E_g}{2k_B T}} \tag{2}$$

$$N_V = 10^{-pH}\, N_A\, 10^{-3} e^{\frac{E_g}{2k_B T}} \tag{3}$$

TCAD Modelling of MoS_2 and WSe_2

MoS_2 and WSe_2 were defined as user-defined materials in Silvaco ATLAS with silicon as the base. The material parameters used for modeling them are provided in Supplementary Table 2. Schottky contacts were defined on both materials with a barrier height and contact resistance (R_S = R_D = $R_C/2$). Barrier lowering was enabled to model image force lowering of the Schottky barrier. Both thermionic and tunneling transport are also enabled on these contacts using the universal Schottky tunneling model (UST).[10] The low-field carrier mobility in each material is defined using the Arora

model.[9,10] This model defines both temperature and doping dependent mobility in the semiconductor.

For initial calibration, parameters such as mobility, Schottky barrier height, and contact resistance were adjusted to approximately match the simulated device currents with the experiment data. Later, interface trap charges were introduced to match the subthreshold characteristics. Acceptor traps were introduced at HfO_2 – MoS_2 interface and affects the subthreshold characteristics of n-channel regime of operation. Similarly, donor traps were added to MoS_2-WSe_2 interface to match the p-channel regime of operation. The energy levels and the trap density were determined by iterating for the best possible fit for transfer characteristics and is tabulated in Supplementary Table 3.

Supplementary References

1. Li, H., Wu, J., Yin, Z. & Zhang, H. Preparation and applications of mechanically exfoliated single-layer and multilayer MoS_2 and WSe_2 nanosheets. *Acc. Chem. Res.* **47**, 1067–1075 (2014).
2. Gusakova, J. *et al.* Electronic Properties of Bulk and Monolayer TMDs: Theoretical Study Within DFT Framework (GVJ-2e Method). *Phys. status solidi* **214**, 1700218 (2017).
3. Jin, Z., Li, X., Mullen, J. T. & Kim, K. W. Intrinsic transport properties of electrons and holes in monolayer transition-metal dichalcogenides. *Phys. Rev. B - Condens. Matter Mater. Phys.* **90**, 045422 (2014).
4. Xiao, J., Zhang, Y., Chen, H., Xu, N. & Deng, S. Enhanced Performance of a Monolayer MoS_2/WSe_2 Heterojunction as a Photoelectrochemical Cathode. *Nano-Micro Lett.* **10**, 1–9 (2018).
5. Yu, C. H., Su, P. & Chuang, C. Te. Impact of Random Variations on Cell Stability and Write-Ability of Low-Voltage SRAMs Using Monolayer and Bilayer Transition Metal Dichalcogenide (TMD) MOSFETs. *IEEE Electron Device Lett.* **37**, 928–931 (2016).
6. Laturia, A., Van de Put, M. L. & Vandenberghe, W. G. Dielectric properties of hexagonal boron nitride and transition metal dichalcogenides: from monolayer to bulk. *npj 2D Mater. Appl.* **2**, (2018).
7. Sanjay, S., Sahoo, K. & Bhat, N. Alcohol-Based Sulfur Treatment for Improved Performance and Yield in Local Back-Gated and Channel-Length-Scaled MoS_2 FETs. *IEEE Trans. Electron Devices* **67**, 3711–3715 (2020).
8. Smyth, C. M. *et al.* Engineering the Palladium−WSe_2 Interface Chemistry for Field Effect Transistors with High-Performance Hole Contacts. *ACS Appl. Nano Mater.* **2**, 75–88 (2019).

9. Arora, N. D., Hauser, J. R. & Roulston, D. J. Electron and Hole Mobilities in Silicon as a Function of Concentration and Temperature. *IEEE Trans. Electron Devices* **29**, 292–295 (1982).
10. Silvaco Inc. *ATLAS User's Manual: Device Simulation Software*. *Silvaco Int., Santa Clara, CA* (2016).
11. Mohammadi, E. & Manavizadeh, N. An Accurate TCAD-Based Model for ISFET Simulation. *IEEE Trans. Electron Devices* **65**, 3950–3956 (2018).
12. Pittino, F., Palestri, P., Scarbolo, P., Esseni, D. & Selmi, L. Models for the use of commercial TCAD in the analysis of silicon-based integrated biosensors. *Solid. State. Electron.* **98**, 63–69 (2014).